ELSEVIER

International Journal of Heat and Fluid Flow 23 (2002) 444–454

International Journal of HEAT AND FLUID FLOW

www.elsevier.com/locate/ijhff

Development of a low Reynolds number enhanced heat transfer surface using flow visualization techniques

J.-H. Ko, M.E. Ewing [1], Y.G. Guezennec *, R.N. Christensen

Mechanical Engineering Department, Ohio State University, 206 W 18th Avenue, Columbus, OH 43210, USA

Received 23 October 2000; accepted 9 October 2001

Abstract

In this paper, an extensive flow visualization study was conducted to design and optimize a heat transfer surface suitable for compact heat exchangers operating in a low Reynolds number regime. The design of the new surface was achieved by carefully identifying possible enhancement mechanisms and choosing a geometry, which would promote these effects at lower Reynolds numbers than other enhanced surfaces. The new geometry, referred to here as a "pin–fin", provides excellent transport characteristics by generating strong, unsteady, and three-dimensional vorticity under all flow conditions. © 2002 Elsevier Science Inc. All rights reserved.

1. Introduction

This paper details the development and optimization of a low Reynolds number heat transfer surface to be used as an enhanced fin in a compact heat exchanger operating in the low Reynolds number flow regime. By Reynolds number, we will be referring throughout this paper to the Reynolds number based on the hydraulic diameter of the individual flow passages, as it is customarily done. Most compact heat exchangers are designed and have been optimized for flow conditions characterized by relatively large Reynolds numbers (1000 and above, typically) for which the fin designs are particularly efficient at providing enhanced heat transfer over conventional plain fins. A very large number of studies have extensively dealt with this topic (see Kays, 1972; Sparrow et al., 1977; Kajino and Hiramatsu, 1987; Aoki et al., 1989; Suga and Aoki, 1991; Sahnoun and Webb, 1992; Goldstein and Sparrow, 1977; O'Brien and Sparrow, 1982; Sparrow and Hossfeld, 1984) and have resulted in a wide array of manufactured products. Tabulated data as well as empirical correlation and design guides have been collected for a large number of surfaces over the years. Careful review of this available data reveals two relatively universal facts. The heat transfer performance of all these surfaces degrades considerably as the Reynolds number decreases; and consequently, very little data are available in the low Reynolds number regime, as clearly these surfaces are not suited for this operating range. However, there are engineering applications where the designer cannot operate the heat exchanger in a favorable flow regime and enhanced heat transfer surfaces specifically optimized for these low Reynolds numbers are called for. The specific application which motivated the current study is the design and optimization of a number of air-cooled heat exchangers for a very high altitude, subsonic atmospheric sampling plane (NASA ERAST program). In this specific application, the flow speeds are not small, but the very high targeted altitude (in the range of 80,000–90,000 ft) results in very small air density, and resultantly low Reynolds numbers for the heat exchangers (Bents et al., 1996). In this application it is expected that Reynolds number of the order 50–100 may be encountered at the low end, which is typically one order of magnitude lower than most available data on heat exchanger performance. Furthermore, all the available data show a rapid deterioration of the heat transfer characteristics as the Reynolds numbers are reduced below 500 or 1000.

* Corresponding author. Tel.: +1-614-292-1910; fax: +1-614-292-3163.

E-mail address: guezennec@osu.edu (Y.G. Guezennec).

[1] Currently with ATK Thiokol Propulsion, Brigham City, UT, USA.

PII: S0142-727X(01)00140-0

Prior to embarking on the design of a low Reynolds number enhanced heat transfer surface, it is important to understand the various mechanisms at play in traditional surfaces, to identify the flow phenomena responsible for that enhancement, and the degradation of these phenomena at low Reynolds numbers. This, in turn, will allow a surface to be "crafted" with features which will best embody those (or other) concepts at much lower Reynolds numbers. In the next few paragraphs, a brief review of traditional families of enhanced surfaces will be carried out.

In addition to providing increased surface area, extended surfaces (or fins) augment heat transfer through the promotion of beneficial flow patterns that increase the local heat transfer coefficient. Of the several types of fins that are commercially available, almost all can be characterized in three broad families: offset-strip fins, louvered fins, and wavy fins. The flow-related enhancements for these fins are always associated with one of the following two mechanisms (Webb, 1994):

1. Boundary layer disruptions (renewal, separation/reattachment).
2. Bulk mixing through secondary flow patterns.

The offset-strip fin is one of the oldest and most widely used types of enhanced surfaces for compact heat exchangers. Offset-strip fins augment the local heat transfer coefficients through repeatedly interrupted flow passages that create successive entrance regions. The boundary layers are then shed and dissipated in the wake region, resulting in the formation of new boundary layers in the downstream channels. This constant boundary layer renewal results in a very large increase in the local heat transfer coefficient, and hence the overall performance. Degradation in performance occurs with reduced Reynolds numbers due to the natural growth of the boundary layers and the increasing sensitivity of the fin leading edges to local boundary layer separation. Furthermore, manufacturing limitations constrain the shortness of the fins, thereby limiting conditions for which the fins are designed. Flow visualization studies have also revealed secondary enhancement mechanisms associated with three-dimensional flow patterns resulting from vortex shedding and oscillations in the wake regions of the fins (Joshi and Webb, 1987). However, these flow patterns and the related heat transfer enhancement (by bulk mixing) are suppressed as Reynolds numbers are reduced to values below approximately 1000 (Joshi and Webb, 1987; Ewing, 1997).

Louvered fins are widely used in the automotive industry. Practically all automotive radiators use this type of fin. The success of this geometry is mainly associated with manufacturability; louvered fins are made in a rolling process that can produce fins about 10 times faster than the stamping process usually required for offset-strip fins. Enhancement for this type of fin is associated with renewed boundary layers over the louvers as well as three-dimensional patterns resulting from flow redirection by the louvers. Therefore, the enhancement is reliant upon a significant portion of "louver directed" flow (Webb and Trauger, 1991). Several studies (Davenport, 1983; Achaichia and Cowell, 1988; Webb and Trauger, 1991; Ewing, 1997) have revealed a transition from a "louver directed" flow to a "duct directed" flow which bypasses the louvers as the Reynolds number is decreased. In this mode, the flow entirely separates over the louver surfaces, resulting in duct flow between the crests of the louvers. This flow transition significantly decreases the heat transfer while increasing the pressure drop, making the louvered fin a poor performer at reduced Reynolds numbers (Ewing, 1997). While the phenomenon can be controlled to some extent by the fin spacing (fin pitch), at very low Reynolds numbers, all practical louvered fin geometries are significantly affected by this phenomenon (Ewing, 1997).

Wavy fins use a much less aggressive form of flow modification than the offset-strip and louvered types. As a result, both heat transfer and friction factors are lower for this type of surface (Ewing, 1997). Unlike the other two types of fins cited above, the wavy fins rely primarily on increased surface area per unit length and the periodic thinning/thickening of the boundary layer as the bulk flow is forced to meander through the troughs and crests. This induces periodic cross-stream momentum and heat transfer, hence enhancing the convection of heat away from the surfaces. The wavy fins are also susceptible to degradation in flow performance at low Reynolds numbers as permanent separation regions occur, especially with large fin spacings, in the crests and troughs (Sparrow and Comb, 1983; Molki and Yuen, 1986; Ali and Ramadhyani, 1992; Ewing, 1997).

In low Reynolds number applications, care must be taken to select the appropriate type of fin and the fin parameters. As indicated above, improper selection of an enhancement technique may result in flow separation and stagnation regions which degrade heat transfer while augmenting pressure drop, resulting in performance that is inferior to even a non-enhanced fin. The present paper focuses on the need to develop a surface with sustained performance at reduced Reynolds numbers. The purpose of this paper is to develop and optimize a new heat transfer surface suited for this flow regime, focusing solely on the understanding and enhancement of the fluid transport mechanisms. In a second phase to be reported elsewhere (see also Ewing, 1997), the measured heat transfer characteristics of the newly crafted surface will be presented and discussed. In essence, in this paper we are attempting to showcase a fluid mechanics-based design methodology for developing a surface capable of providing significantly

enhanced transport characteristics (in this case heat transfer) in a specific range of flow parameters typically associated with laminar flows with poor transport characteristics.

2. Surface development

By examining the various flow enhancement mechanisms associated with traditional enhanced fins at higher Reynolds number, we identified a number of desirable characteristics for the new surface (Ko, 1997; Ewing, 1997):

1. The surface should promote three-dimensional flow activity, even at reduced Reynolds numbers.
2. The surface should provide periodic boundary layer disruptions, even at low Reynolds numbers.
3. The surface should not promote steady, large-scale separation at low Reynolds numbers, as is seen in the louvered and wavy type surfaces.
4. The flow geometry should be relatively open to reduce pressure drop penalties.

Low Reynolds number flows are in general ineffective as the transport is primarily diffusion-controlled. At high Reynolds numbers, turbulent or transition flows are different, as the dominant transport mode, especially at large distances, is convective in nature, with diffusion only acting at small scales where it can be effective. Generically, one of the key characteristics of turbulence is the presence of strong three-dimensional vortical motions (turbulent eddies), even when the mean vorticity (boundary-induced, usually) is only along one or two directions. Furthermore, the vorticity in turbulent flow is not distributed (such as in the boundary layer shear), but is actually concentrated in space and leading to strong secondary (cross-stream) motions. Hence, we attempted to craft a surface that would best embody these flow features. The resulting surface is referred to here as a "pin–fin" surface, and is schematically illustrated in Fig. 1. The geometry consists of a plain rectangular fin surface with a series of pins passing through the fins, transverse to the flow direction. This configuration was chosen to best meet the characteristics listed above, as it was expected to provide the following enhancement mechanisms (Ko, 1997; Ewing, 1997):

1. Regions of high heat transfer coefficients in the renewed (thin) boundary layers near the stagnation region of each pin.
2. Creation of transverse vorticity in the wake regions of the pins, possibly rolling into discrete vortices.
3. Forced meandering of the bulk flow between the staggered array of pins, i.e. a fluidic equivalent of wavy fins in the transverse direction, without the surfaces.
4. Spatially concentrating the distributed boundary layer vorticity (mean flow vorticity/shear) on the fins by rolling it into discrete vortices upstream of the pin/fin junction, hence inducing strong transport normal to the fins.
5. Amplification of this localized vorticity by a "wrapping and stretching" of the stagnation vortex into a horseshoe vortex around the pins. This results in vortices now aligned in the streamwise direction on either side of the pins, also contributing to transport in the direction normal to the fins.
6. Possible phase-locking in the wake regions of the pins to promote vortex shedding at low Reynolds numbers.

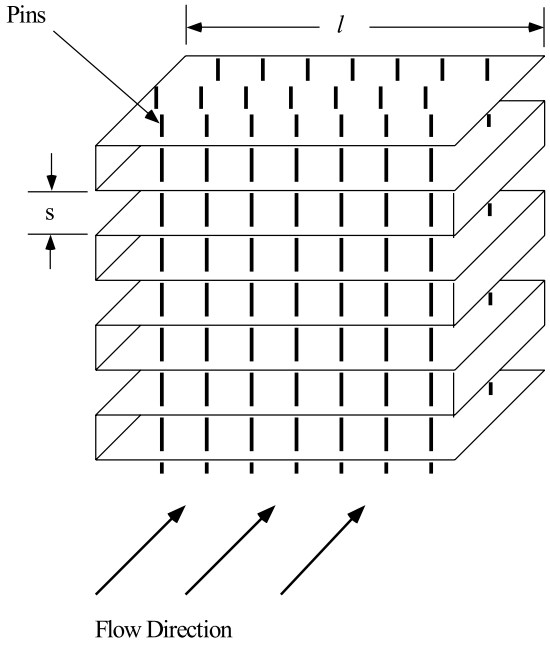

Fig. 1. Illustration of the pin–fin geometry.

Hence, by this arrangement, strong vorticity along all three axes is induced, and furthermore, these three components are forced to interact due to their localized sources in close proximity. Therefore, the pin–fin geometry was designed to intrinsically force three-dimensional flow patterns and boundary layer disruptions, which are the missing characteristics of most low Reynolds number flows.

Within this family of surfaces designed to promote the desired flow characteristics, it is then necessary to optimize the various geometrical parameters to achieve the highest transport enhancement, at the lowest cost in terms of pressure drop. Specifically, three geometrical parameters were investigated: the planar arrangement of the pins (streamwise and spanwise spacing), and the fin

spacing in the transverse (normal) direction. The parameters effectively control the spatial concentration of the aforementioned effects in all three directions. From the transport standpoint, it is desirable to concentrate the sources of vortical activity, particularly at low Reynolds numbers where the effects are relatively short lived and dissipate quickly. On the other hand, these sources of vorticity are also associated with flow obstructions, and hence pressure drop along the main flow direction. The "optimal" surface is a compromise between these two aspects. To that effect, a parametric study was performed using flow visualization techniques in scaled-up models, to provide insights into the optimal trends in the fin parameters.

Referring to Fig. 1, key parameters for the new surface are the fin spacing (s), the fin length (l), the pin diameter (d), and the pin placements within the pin array. The general shape of the flow passage can be characterized by the channel aspect ratio, defined as s/l. Small aspect ratios are desirable from the standpoint of increased heat transfer area and increased compactness. However, practical limitations are imposed on this parameter; fin efficiencies diminish with increasing fin length (l) while flow resistance, with associated suppression of turbulent flow features, increases with decreased spacing, s. Typical aspect ratios for the fins of compact heat exchangers range from 0.1 to 1.0 (see, for example, the several plate-fin surfaces described in Kays and London, 1997). The primary challenge for the application motivating the present study, heat exchangers for the high altitude aircraft previously described, was the reduction of heat exchanger frontal area. Accordingly, heat transfer surfaces with small aspect ratios were desired. The challenge was then to develop the surface with small aspect ratios while maintaining favorable flow characteristics at the reduced Reynolds numbers. Aspect ratios toward the lower end of the typical values were targeted, and the three values of 0.1, 0.15 and 0.2 were selected as candidates.

Small pin diameters were desired to decrease the scale of flow separation regions downstream from the pins. Manufacturing considerations limited the lower range of practical pin diameters; the anticipated manufacturing technique was to mechanically drive the pins through the fins, using dies to guide the pins into position. It was determined that the required pin diameter would be of the order of 1.27 mm (0.050 in.), and the diameter of the scaled-up model corresponded to this value. [2]

[2] Actual manufacturing of the heat exchanger fins was accomplished using 0.76 mm (0.030 in.) pins. The resulting surface, along with thermal and hydraulic performance characteristics, is described in a separate manuscript currently in preparation.

3. Description of experiments

The investigation of the flow characteristics in the various geometries was carried out using detailed flow visualization over a wide array of conditions. Since, in a typical heat exchanger, the flow passages are very small, the flow visualization was carried out using scaled-up models in a water channel. In all the experiments, the Reynolds number (based on the flow passage hydraulic diameter, in the conventional fashion) was matched between the actual scale and operating flow rates in air, and the water channel experiments. Owing to the difference in viscosity for the working fluid (water vs. air) and the 15:1 geometrical scale of the models, the flow speeds were considerably reduced while matching the Reynolds numbers. This methodology has been extensively used in many flow visualization studies for all kinds of flow situations (Clayton and Massey, 1967; Merzkirch, 1987). The scaled-up models as well as the low fluid velocities allow very detailed flow characterization to be carried out, as well as easy recording with conventional photographic techniques.

3.1. Flow facility

The flow visualization was performed in a transparent water channel. The facility consisted of a closed-loop water channel that accommodated scaled-up acrylic models of heat exchanger surfaces. The facility is schematically shown in Fig. 2. The water channel was made of transparent acrylic with a 0.3×0.3 m^2 (1×1 ft^2)

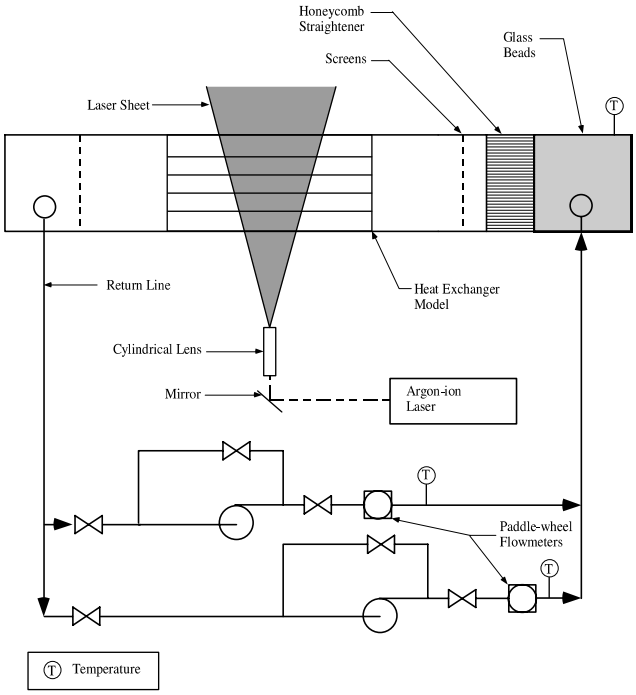

Fig. 2. Schematic diagram of the flow visualization facility.

cross-sectional area. The overall length of the channel was approximately 1.8 m (6 ft). The flow speeds were adjustable over a wide range by a combination of valves, typically allowing visualization in the scaled-up arrays of heat exchanger surfaces in the nominal Reynolds number range of 50–3000 (based on the hydraulic diameter of the model). Two flow meters constantly monitored the flow rate in the channel, and the water temperature (nominally ambient) was recorded during each test. The flow was conditioned upstream of the test section by a packed bed of spheres, followed by screens and a honeycomb straightener to ensure a low level of turbulence and a uniform velocity profile in the test section.

In order to carry out the flow visualization, the water was seeded with small, (almost) neutrally buoyant particles (90–150 μm in diameter, typically). The particles were illuminated with a laser sheet from a 5 W Ar^+ continuous-wave laser. The laser sheet was formed using mirrors and a cylindrical lens under the channel and passed vertically through the transparent bottom of the channel. The sheet-forming optics and mirrors were placed on a small translation stage to allow easy adjustment of the laser sheet position with respect to the model. The models were also made of transparent acrylic material to allow the laser sheet to illuminate the flow field throughout the model. Owing to small density differences between the particles and the water, and the very low flow speeds used at the low end of the Reynolds number range, a small quantity of sugar was added into the water to match the specific gravity of the particles as exactly as possible. In order to account for the presence of the sugar, samples of the water/sugar weak solution were collected and their specific gravity and viscosity were measured using a viscometer as a function of temperature in order to appropriately calculate the Reynolds numbers for each case tested.

The flow visualization was observed through the side of the flow channel, perpendicular to the laser sheet. Two modes of recording for the flow visualization were used: static recordings using a 35 mm camera (photographs shown later in this paper), and extensive video recordings of the dynamics of the flow patterns. In the 35 mm camera case, the shutter speed was adjusted to record short streaks of the particle trajectories in order to best capture the key features of the flow patterns. In the video mode, the dynamics of the flow were documented with an editing S-VHS recorder and a CCD camera. For all the flow conditions and models, video sequences of at least 2 min of duration were always recorded to provide ample details of the flow behavior. All the conclusions reached in this paper were obtained based on the detailed analysis of the video sequences. On that basis, a set of static photographs was selected to best represent the underlying phenomena. This must be kept in mind, as some of the mechanistic understanding of the flow fields described in the following sections is best observed in the dynamics (or lack of) in the flow.

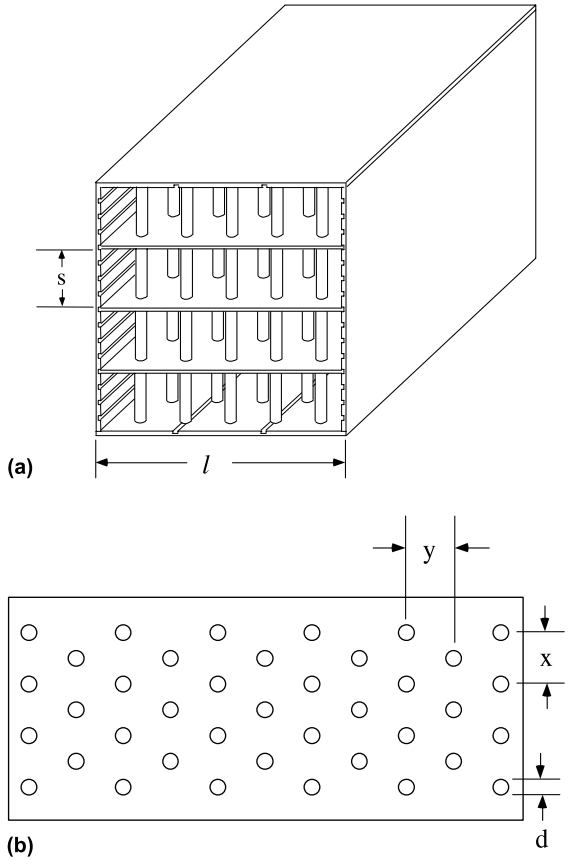

Fig. 3. Pin–fin model geometry: (a) pin–fin model assembly and (b) pin arrangement for the pin–fin model.

3.2. Models

The pin–fin models were constructed with transparent thin (2 mm) acrylic sheets and tubes. The sheets, which represented the fins, were positioned inside an enclosure as shown in Fig. 3(a). The enclosure was approximately 90 cm (3 ft) in length and its cross-section fits exactly in the test section of the water channel. It could be rotated on its side to allow the flow visualization in both the horizontal and vertical (fin) orientations, as will be described below. The enclosure had several grooves (3 mm in depth) machined in the sides to allow variation of the fin spacing in a modular fashion. Holes were cut into the thin sheets (fins) to accommodate the 19 mm (0.75 in.) diameter acrylic tubes, which represented the anticipated 1.27 mm (0.050 in.) diameter pins at the 15:1 scale factor.

Three different pin arrangements were considered to study the effects of pin spacing on the resulting flow characteristics. In addition, for each pin configuration, the fin spacing was also varied by inserting more fins into the enclosure. As described in the previous section,

Table 1
Parameters for the pin–fin arrangements

Model	s (mm)	l (mm)	s/l	y (mm)	x (mm)	s/d	x/d	y/d
PFA-S2	28.6	292.1	0.10	73.9	73.9	1.5	3.88	3.88
PFA-S3	44.5	292.1	0.15	73.9	73.9	2.33	3.88	3.88
PFA-S4	60.3	292.1	0.21	73.9	73.9	3.17	3.88	3.88
PFA-S2	28.6	292.1	0.10	49.3	73.9	1.5	2.59	3.88
PFA-S3	44.5	292.1	0.15	49.3	73.9	2.33	2.59	3.88
PFA-S4	60.3	292.1	0.21	49.3	73.9	3.17	2.59	3.88
PFA-S2	28.6	292.1	0.10	49.3	49.3	1.5	2.59	2.59
PFA-S3	44.5	292.1	0.15	49.3	49.3	2.33	2.59	2.59
PFA-S4	60.3	292.1	0.21	49.3	49.3	3.17	2.59	2.59

aspect ratios, defined as s/w (see Fig. 1), of 0.1, 0.15 and 0.20 were targeted. Fig. 3(b) illustrates the parameters used to characterize the geometry, namely, the fin spacing, s, the fin length, w, the pin diameter, d, the pin streamwise spacing, y, and the spanwise spacing, x. In all, nine combinations of pin arrangements (A, B and C) and three fin spacings (S2, S3 and S4) were investigated, as summarized in Table 1. The different spacings for

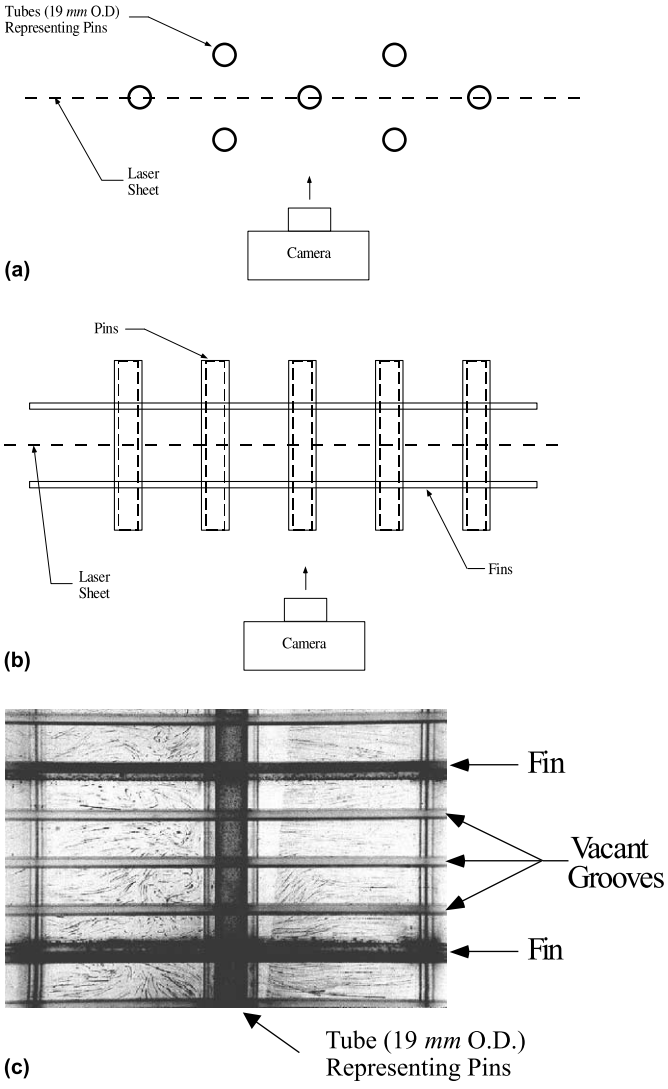

Fig. 4. View orientation for flow visualization photographs: (a) "vertical" view (pins appear vertical in the photographs); (b) "horizontal" view (cross-section of the pins are seen in the photographs) and (c) illustration of fins and grooves in vertical view.

each model correspond to two, three, and four spacings between the grooves in the enclosure, and are labeled, S2, S3, and S4, respectively.

As mentioned earlier, the flow visualization was carried out in two different orientations, achieved by rotating the entire model in the test section with respect to the laser sheet and camera. Figs. 4(a) and (b) illustrate the two visualization orientations, namely a "vertical" view (Fig. 4(a) where the pins are vertical (and the fins horizontal and parallel to the camera axis) and an "horizontal" view (Fig. 4(b)) where the pins are horizontal (parallel to the camera axis) and the fins are vertical. The "vertical" view was mostly used to visualize the transport mechanisms normal to the fins and to study the effects of the fin spacing, while the "horizontal" view was mostly used to document the cross-stream transport and mixing parallel to the fin surface and study the effects of the pin configuration. In both views, the location of the laser sheet was varied to better understand the complex, three-dimensional flow patterns created by this geometry. In the "vertical" view, the laser sheet was placed both aligned with the row of pins (as shown in Fig. 4(a)), and between the row of pins. In the "horizontal" view, the laser sheet was placed both at the mid-plane between fins (as shown in Fig. 4(b)), and close to the fin surface. Fig. 4(c) shows a typical photograph of the flow field in the "vertical" view. The dark lines near the top and bottom of the photograph correspond to the fin position. The three additional gray lines in the center correspond only to the visual obstruction created by the vacant grooves located on the side of the model enclosure. They do not correspond to any physical surface within the flow field and the entire region of the flow between the fins is occupied by the fluid. It should be noted that these small vacant grooves (3 mm deep, out of 30 cm flow width) have a very minimal impact on the flow field and their interference in the photographs is strictly visual.

4. Results

As described earlier, a very extensive flow visualization study was carried out to characterize and optimize the pin–fin surface. In total, nine different surfaces were tested, corresponding to three pin arrangements for three different fin spacings each. For each of these cases, flow visualization was conducted over a wide range of Reynolds numbers. The Reynolds number is based on the hydraulic diameter, D_h, which is based on the flow cross-section, excluding the pins. Referring to Fig. 3(a), D_h is then $2ls/(l+s)$.

For each flow condition, the flow was examined with two laser sheet positions for both "vertical" and "horizontal" views. Approximately 15 h of video recordings and hundreds of photographs were taken to document all these flow conditions and geometries. These photographic and cinematographic records were thoroughly reviewed to develop a firm understanding of the details of the transport phenomena and to select the most promising geometry for a heat exchanger surface capable of surpassing all the existing enhanced heat transfer surfaces in the low Reynolds number regime, while maintaining good performance in the high Reynolds number range. The paragraphs below provide only a synopsis of the extensive results obtained. A more extensive collection and discussion of the results can be found in Ko (1997). In this section, the results will be organized as follows. First, the generic flow features of the pin–fin surface will be described to demonstrate that the targeted flow transport phenomena (outlined earlier) have been achieved. Then, the effects of pin arrangement and fin spacing will be presented. Finally, the configuration deemed optimal for the targeted application will be presented.

4.1. Generic flow features of the pin–fin geometry

Fig. 5 illustrates the typical flow features observed with the pin–fin geometry in the horizontal (Fig. 5(a)) and vertical (Fig. 5(b)) views, respectively. These specific photographs have been chosen to best depict the flow

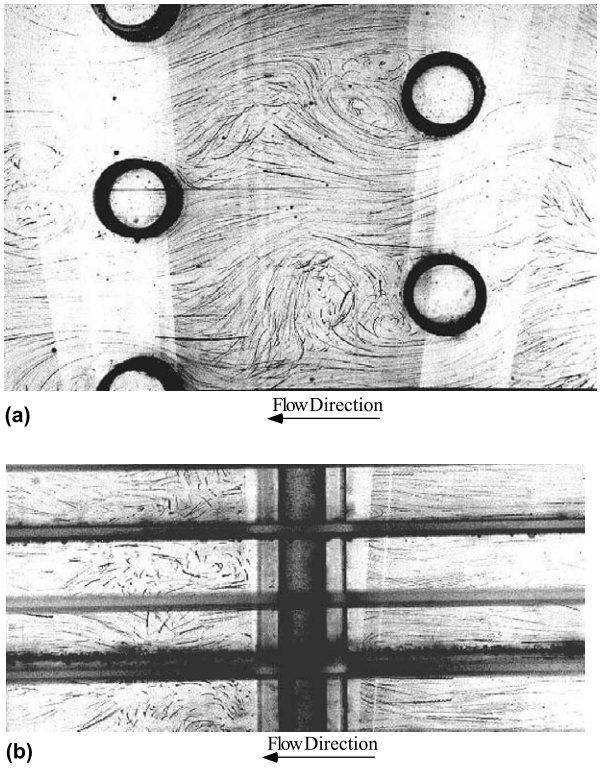

Fig. 5. Typical flow features: (a) horizontal view (model PFB-S4, $Re = 730$) and (b) vertical view (model PFA-S2, $Re = 740$).

features present in this generic geometry. However, the two photographs are not taken for the same case (pin arrangement "B" and spacing "S4" vs. pin arrangement "A" and spacing "S2"). Furthermore, these photographs correspond to an intermediate Reynolds number (around 750) to best illustrate the phenomena. Comparative photographs taken with the various geometries at low Reynolds number will be shown in the next few paragraphs.

All the observations confirmed the existence of the desired flow patterns. As can be seen in Fig. 5, the patterns are highly three-dimensional. In the horizontal view (Fig. 5(a)), the mean flow field meanders between the staggered array of pins as it would in a wavy fin, without the frictional drag associated with the solid surfaces. Furthermore, due to the periodic presence of the pins and the related change in flow cross-section, the mean flow accelerates over each row of pins and decelerates in between, providing additional sources and sinks of vorticity. Of course, downstream of the pins, the flow separates from the pins in the wake region, providing a strong source of vorticity aligned with the pins. At high and moderate Reynolds numbers, these wakes are shed periodically, as they would behind an isolated cylinder. However, at low Reynolds numbers, this quasi-periodic shedding persists longer than it would with isolated cylinders, as the periodic array of pins is more globally unstable and the wakes are phase-locked. In any case, whether steady or unsteady, the wake regions downstream of each pin act as a large source of vorticity with one specific orientation (parallel to the pins). In the vertical view (Fig. 5(b)), the flow exhibits many favorable characteristics. Upstream of the pins, near the pin/fin junctions the distributed vorticity present in the "channel flow" created between the fins is rolled up into a localized horseshoe vortex, as expected. Due to the flow acceleration around the pins, these vortices are wrapped around, stretched and amplified, and provide strong pairs of counter-rotating vortices (axial vorticity). On the downstream side of the pin, the flow is complex and highly three-dimensional. While the streamwise velocities in the separated wake regions are relatively small, the strong spanwise components are expected to provide significant heat exchange between the fin surfaces and the bulk fluid stream. This can be attributed to the strong interaction of concentrated vorticity along all three directions: the wake vortices (normal to the fins), the counter-rotating (axial) vortices arising from the horseshoe vortices, and the background vorticity associated with the mean shear between the fins. Hence, as targeted, this geometry induces strong "seeds" of three-dimensional vorticity (typical characteristics of high Reynolds numbers, turbulent flows), even at low Reynolds numbers. It is important to note that, from a transport standpoint (heat transfer, in this case), there is considerable scalar transport normal to the fins, hence providing enhanced bulk mixing.

One additional flow feature is to be noted in these photographs: At moderate to low Reynolds numbers, despite the strong sources of vortical transport, the flow re-laminarizes after some distance downstream. Hence, the pin placement and the fin spacing play an important role in providing the overall desired mixing characteristics to maintain good bulk mixing by controlling the "seeding density" of mixing regions. This optimization aspect will be examined in the next few paragraphs.

4.2. Effect of pin configuration and fin spacing

Fig. 6 shows a comparison of the flow features among three different pin arrangements, namely arrangements "A", "B" and "C" (see Table 1) for the same fin spacing ("S4") at similar Reynolds numbers (relatively low) in

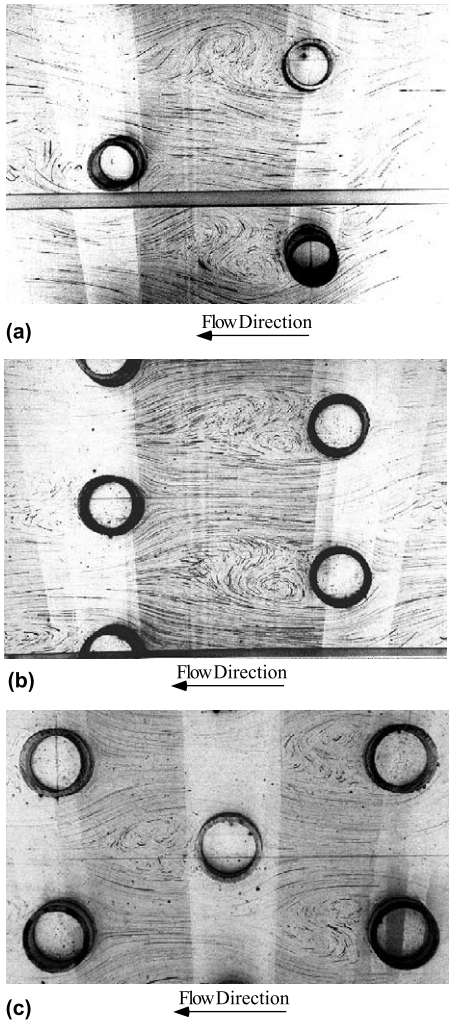

Fig. 6. Effect of pin configuration in horizontal view: (a) PFA-S4 model, $Re = 225$, (b) PFB-S4 model, $Re = 225$ and (c) PFC-S4 model, $Re = 330$.

the horizontal view. Similar results and trends were observed with the other fin spacings (not shown here, for brevity). As described earlier, the flow fields for these three cases are characterized by strong separations in the wake of the pins and significant meandering of the bulk flow between the pins and their wakes. Pin arrangement "A" represents the most open geometry. For pin arrangement "B", the streamwise spacing is kept the same as for arrangement "A", but the spanwise spacing is reduced by one-third. For pin arrangement "C", the spanwise spacing is the same as for arrangement "B", but the streamwise spacing is also reduced by one-third. Hence, the flow blockage increases progressively from configuration "A" to "B" to "C".

Fig. 6(a) depicts the flow pattern with the "A" configuration (the most open geometry). As observed in this figure, the wakes are rather unconstrained in the plane of the figure, expanding to widths in excess of the pin diameter as they would with isolated cylinder wakes in a large area. While at this relatively low Reynolds number the downstream extent of the wakes is not very large, it appears that the wakes persist at least until the next row of pins. Furthermore, the time history of the flow captured in the videotapes shows that these wakes are still unsteady (quasi-periodic) at this relatively low Reynolds number. This contributes to a significant "modulation" of the stagnation regions of the next row of pins and presumably a "phase-locking" of the wakes from the array of pins leading to maintaining the vortex shedding at low Reynolds numbers.

Fig. 6(b) illustrates the flow in the "B" configuration (intermediate pin density). While this more compact pin arrangement offers more "seeds" of vorticity per unit area, the flow is more strongly accelerated in between the pins due to the higher geometrical blockage, resulting in a "quenching" of the wakes downstream of the pins. This "quenching" takes two forms: First, the lateral extent of the wakes becomes reduced, and second, there is a suppression of the unsteady wake oscillations and the related mixing phenomena at low Reynolds numbers. However, the downstream persistence of the two-dimensional wakes appears to be relatively unaffected, extending to the next row of pins.

This trend of increased suppression of the wakes with increased pin density is also confirmed in the "C" configuration (the densest geometry), as seen in Fig. 6(c). Here, the strong meandering of the bulk flow between the pins tends to re-laminarize immediately downstream of the initial wake regions and also prevents the periodic shedding of the wake vortices. While the videotapes show that the wake vortices are highly active and concentrated, the lack of shedding of these vortices contributes to steady recirculation zones, which are likely to be detrimental to the heat transfer enhancement.

Fig. 7 depicts a comparison of the flow features among the different fin spacings with the most promising

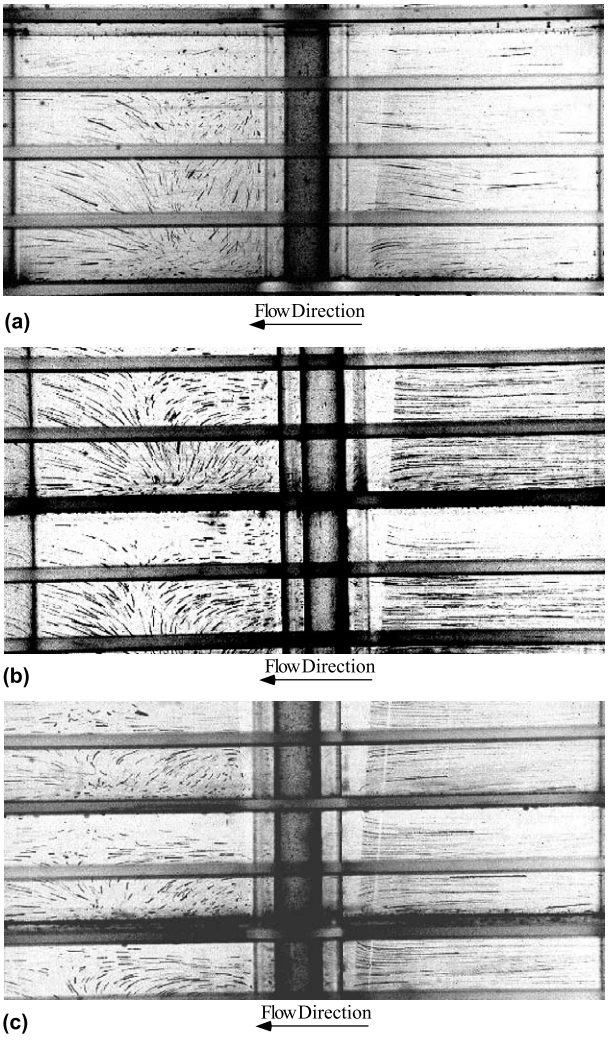

Fig. 7. Effect of pin configuration in vertical view: (a) PFA-S4 model, $Re = 230$, (b) PFA-S3 model, $Re = 240$ and (c) PFA-S2 model, $Re = 390$.

pin placement (arrangement "A"), as seen in the preceding paragraphs. The effect of the fin spacing is best illustrated in the "vertical" view which shows the transport in the direction normal to the fins. As described earlier, one of the generic flow features of the pin–fin geometry is to promote the creation of a strong pair of counter-rotating streamwise vortices (emanating for the horse-shoe vortices at the pin–fin junctions) and have them strongly interact with the wake vortices downstream of the pins. In that sense, the fin spacing determines directly the two-dimensionality (or lack of) of the wakes and the level of three-dimensional transport generated downstream of the pins. In Fig. 7(a), the fin spacing is the largest ("S4") with the fins (dark gray lines) located at the very top and bottom of the photograph. In Fig. 7(b), the fin spacing is intermediate ("S3") with the fins located near the center and right below the very bottom of the photograph. In Fig. 7(c), the fin

spacing is the smallest (''S2'') with the fins located at 1/3 and 1/4 height in the photograph.

The presence of the horseshoe vortex upstream of the pins is clearly visible for all the three fin spacings. The diameter of that vortex is essentially constant for all the spacings. This means that the upstream flow is strongly affected by these vortices with the smallest spacing (Fig. 7(c)), while the center of the flow remains relatively unaffected in the largest spacing case. Despite these upstream differences, the strong interaction between the wakes of the pins and these wrapped-around vortices in the downstream region creates a strong mixing in all the cases. This strong mixing region located in the base region of the wakes of the pins is a strong contributor to the transport away from the fins. The presence of this sustained, extensive cross-stream transport to and from the fins shows the advantage of this pin–fin geometry over other traditional heat transfer surfaces. Hence, it is desirable that this mixing transports the fluid from the immediate vicinity of the fins to the center region of the flow channel. This type of transport is clearly visible in both the largest (''S4'') and the intermediate (''S3'') spacings. The smallest spacing (''S2'') tends to lead to a slightly more stable center region (presumably formed by the close arrangement of four counter-rotating streamwise vortices downstream of the pins). A review of the photographs and the videotapes corresponding to these spacings in the ''horizontal'' view also indicates that the smaller fin spacings (like the denser pin placements described earlier) tend to decrease the streamwise extent of the cross-stream transport phenomena.

4.3. Performance considerations and selection of fin parameters

In summary, the flow visualization results of the various pin–fin parameters (pin placements and fin spacings) have been analyzed in both the horizontal and the vertical view. These assessments only take into account the observed enhanced transport mechanisms, their steadiness or unsteadiness, and their spatial extent. No direct measurement of the heat transfer characteristics was performed here, and the approach chosen was to optimize the flow characteristics which are most likely to provide good heat transfer characteristics in the context of a compact heat exchanger operating at moderate to low Reynolds numbers.

Based on careful observations of the extensive flow visualization records, we concluded that the PFA-S4 model was the most encouraging candidate for optimizing the pin–fin parameters. This model is characterized by the largest pin and largest fin spacing of those tested. It must be kept in mind that the ''best'' surface is not only one that continues to promote good three-dimensional mixing at low Reynolds numbers, but also a surface which can provide this enhancement at the least pressure drop penalty. While closer spacings (in terms of both the pins and fins) provide more ''seeds'' of vorticity per unit volume, the pressure drop is likely to increase dramatically with the reduction in effective flow passage. Furthermore, the smaller spacings tend to ''quench'' or inhibit the phenomena they are attempting to promote. The denser geometries tend to result in less enhanced mixing area due to the suppressed wake regions resulting from the acceleration and decelerations of the bulk flow around the pins and their wakes. It was found that the streamwise extent of the two-dimensional wakes seems to control the size of the region with strong cross-stream (spanwise) transport. The presence of extended regions with significant three-dimensional vortical transport at low Reynolds numbers, clearly a desirable feature of this pin–fin surface, is best realized in the more open geometry.

5. Conclusions

This study led to the design and optimization of a new, enhanced heat transfer surface specifically designed for operation at low Reynolds numbers. This surface is able to generate three-dimensional flow features in this flow regime, which are essential for the heat transport from the fins to the bulk of the fluid. Typically, most enhanced surface geometries lose their effectiveness at moderate to low Reynolds numbers as the enhancement mechanisms are mostly two-dimensional and often lead to steady separation regions detrimental to heat transfer. The new pin–fin surface is able to induce three-dimensional vorticity and good cross-flow mixing, even at very low Reynolds numbers. It was also found that these beneficial effects were decreased at smaller pin and fin spacings, leading to an ''optimal'' geometry generating enough cross-stream mixing without too much ''self-interference'' and too high of a pressure drop.

Furthermore, the pins themselves are likely to contribute to the heat transfer directly. By proper manufacturing, the pin/fin junctions can offer low thermal resistance, and hence the pins provide additional surface area with high heat transfer characteristics in the stagnation regions upstream of the pins.

In summary, the approach taken in this study was to ''craft'' a heat transfer surface based on the underlying fluid transport phenomena, rather than blindly testing a large number of surfaces (as it is often done in the heat exchanger community), and then identifying the enhancement mechanisms.

Acknowledgements

This research was supported under a Grant from NASA Lewis Research Center under the ERAST

program under the technical supervision of David Bents and Ted Mockler. Their support is gratefully acknowledged.

References

Achaichia, A., Cowell, T.A., 1988. Heat transfer and pressure drop characteristics of flat tube and louvered plate fin surfaces. Exp. Thermal Fluid Sci. 1, 147–157.

Ali, M.M., Ramadhyani, S., 1992. Experiments on convective heat transfer in corrugated channels. Exp. Heat Transfer 5, 175–193.

Aoki, H., Shinagawa, T., Suga, K., 1989. An experimental study of the local heat transfer characteristics in automotive louvered fins. Exp. Thermal Fluid Sci. 1.

Bents, D.J., Mockler, T., Maldonado, J., Hahn, A., Cyrus, J., Schmitz, P., Harp, J., King, J., 1996. Propulsion Selection for 85 Kft Remotely Piloted Atmospheric Science Aircraft. Association for Unmanned Vehicle Systems, Orlando, FL.

Clayton, B.R., Massey, B.S., 1967. Flow visualization in water: a review of techniques. J. Sci. Instrum. 44.

Davenport, C.J., 1983. Correlations for heat transfer and flow friction characteristics of louvered fin. In: Heat Transfer – Seattle 1983, AIChE Symposium Series, No. 225, vol. 79.

Ewing, M.E., 1997. Fundamental studies of enhanced heat exchanger surfaces at low Reynolds numbers. Doctoral Dissertation, The Ohio State University, Columbus, OH.

Goldstein, L.J., Sparrow, E.M., 1977. Heat and mass transfer characteristics for flow in a corrugated wall channel. J. Heat Transfer 99.

Joshi, H.M., Webb, R.L., 1987. Prediction of heat transfer and friction in the offset strip fin array. Int. J. Heat Mass Transfer 30, 69–84.

Kajino, M., Hiramatsu, M., 1987. Research and development of automotive heat exchangers. In: Yang, W.J., Mori, Y. (Eds.), Heat Transfer in High Technology and Power Engineering. Hemisphere, Paris.

Kays, W.M., 1972. Compact heat exchangers. In: Ginoux, J.J. (Ed.), AGARD Lecture Series No. 57 on Heat Exchangers, AGARD-LS-57-72.

Kays, W.M., London, A.L., 1997. Compact Heat Exchangers, 3rd ed. Krieger Publishing Company.

Ko, J.-H., 1997. Phenomenological study of a new family of low Reynolds number heat exchangers using flow visualization. M.S. Thesis, The Ohio State University, Columbus, OH.

Merzkirch, W., 1987. Flow Visualization, 2nd ed. Academic Press, New York.

Molki, M., Yuen, C.M., 1986. Effect of interwall spacing on heat transfer and pressure drop in a corrugated-wall duct. Int. J. Heat Mass Transfer 29 (7), 987–997.

O'Brien, J.E., Sparrow, E.M., 1982. Corrugated-duct heat transfer, pressure drop and flow visualization. J. Heat Transfer 104.

Sahnoun, A., Webb, R.L., 1992. Prediction of heat transfer and friction for the louver fin geometry. J. Heat Transfer 114.

Sparrow, E.M., Baliga, B.R., Patankar, S.V., 1977. Heat transfer and fluid flow analysis of interrupted wall channels with applications to heat exchangers. J. Heat Transfer 99.

Sparrow, E.M., Comb, J.W., 1983. Effect of interwall spacing and fluid flow inlet conditions on a corrugated-wall heat exchanger. Int. J. Heat Mass Transfer 26 (7), 993–1005.

Sparrow, E.M., Hossfeld, M., 1984. Effect of rounding protruding edges on heat transfer and pressure drop in a duct. Int. J. Heat Mass Transfer 27.

Suga, T., Aoki, H., 1991. Numerical study on heat transfer and pressure drop in multilouvered fins. In: Lloyd, J.R., Kurosake, Y. (Eds.), Proceedings of the ASME/JSME Joint Thermal Engineering Conference, vol. 4.

Webb, R.L., 1994. Principles of Enhanced Heat Transfer. Wiley, New York.

Webb, R.L., Trauger, P., 1991. Flow structure in the louvered fin heat exchanger geometry. Exp. Thermal Fluid Sci. 4, 205–217.